Available online at www.sciencedirect.com

ScienceDirect

Procedia Structural Integrity 2 (2016) 3098–3108

Structural Integrity Procedia

www.elsevier.com/locate/procedia

21st European Conference on Fracture, ECF21, 20-24 June 2016, Catania, Italy

Fluid Pressurization and Entrapment Effects on the SIFs of Cracks produced under lubricated Rolling-Sliding Contact Fatigue

Simone Ancellotti[a], Matteo Benedetti[a]*, Michele Dallago[a], Vigilio Fontanari[a]

[a]*Department of Industrial Engineering, University of Trento, Via Sommarive 9, 38123 Trento, Italy*

Abstract

Pitting is one of the causes of failure for mechanical components subjected to rolling contact fatigue. In the present article, a FE model is described in which a 2D half-space with an edge crack is affected by a travelling contact load produced by a cylindrical body. The contact load is not approximated as usual by an analytical pressure distribution but the actual mating body is modelled. The presence of lubricant between the mating bodies and inside the crack is taken into account and its effect on the crack is modelled via hydrostatic elements. The lubricant is assumed to be entrapped into the crack by the external body when the latter covers the crack mouth, that is, the crack is sealed by the contact area and not by the contact between the crack faces (fluid entrapment mechanism). The pressure of the fluid is calculated via an iterative procedure by assuming that its volume stays constant inside the crack. Comparisons between this model and the alternative fluid pressurization mechanism have been made. The outcomes suggest that the fluid pressures inside the crack produced by the fluid entrapment mechanism tend to those of the fluid pressurization mechanisms as the crack becomes short.

Keywords: fluid entrapment, fluid pressurization, inclined edge crack, rolling–sliding contact fatigue, stress intensity factors;

1. Introduction

Rolling contact fatigue mechanism is one of the most typical causes of failure of components like: railway wheels, gears, roll bearing and cams. The repeated load cycle on the contact zone could promote initiation and growing of cracks. As result, alternating microdeformations can produce sub-superficial or superficial cracks. In the first case “shelling” is produced by flows, voids or inclusions inside the material structure. The second case, viz. the

* Corresponding author. Tel.: +39 0461282457; fax: +39 0461281977.
E-mail address: matteo.benedetti@unitn.it

10.1016/j.prostr.2016.06.387

topic of this paper, involves the formation and propagation of shallow cracks, also known as “pitting” or “micropitting”. Sub- and superficial cracks can propagate towards the bulk material and also branch upwardly. As the cracks intersect each other or the tip reaches the external surface, the detachment of material comes up. It has been proved that the friction forces, between the two mating bodies, act in favor of the pitting because they move the point of maximum tangential stress closer to the external surface (Sadeghi(2009)). Olver (2005) provides a rich review of this phenomenon. Another peculiarity is the narrow inclination of the shallow cracks respect to the contact surface. It has been proved that the crack tends to propagate in the same direction of the motion of the contact load over the surfaces.

Nomenclature

FE	Finite Elements method
RCF	Rolling Contact Fatigue
LCFM	lubricated crack faces mechanism
PM	pressurization mechanism
ETM	entrapment mechanism
SIF	Stress Intensity Factor
c	crack length
a	Hertzian conctact pressure distribution half-width
E	elastic modulus
FI, FII	dimensionless Mode I and Mode II SIFs
KI, KII	Mode I and Mode II SIFs
p	value of the Hertzian pressure on the surface
p_c	fluid pressure inside the crack
p_{max}	maximum intensity of the Hertzian contact pressure distribution
x	distance of the Herzian load from crack mouth
μ_c	contact surface friction
μ_f	friction between crack faces
Φ	crack inclination angle of the crack respect to contact surface
E	Young’s module
ν	Poisson’s ratio

The representation of the real crack in 2D could be an acceptable compromise between computational cost and accuracy. Normally, 2D model in plane strain conditions is chosen, in lieu of a 3D one, for the sake of simplicity in numerical resolution. In addition, it is also possible to justify this choice by considering that often the crack is shorter than the thickness of the mating bodies. A 2D model is able to simulate adequately the crack problem, in fact, there is no qualitative difference in the results between the 2D (M. Beghini (2004), J. W. Ringsberg (2003), Bower (1988), Keer (1982), Keer (1983), Fletcher (1999), Bogdanski (1996), Bogdanski (1997)) and 3D (Murakami (1985), Kaneta (1985), Kaneta (1987), Bogdanski (2008)) models presented. In addition, 2D results are in general more conservative (Bogdanski (2008)), although this might not be always true and great care must be put into using 2D models for quantitative predictions (Bogdanski (1996)). However, the extension of the crack in 3D space worth to be studied (Fletcher (2008)).

Pitting has been rarely seen in not lubricated (dry) contact conditions; Therefore, the researchers and different literatures (Ren(2002), Ringsberg (2003)) hypothesize that the pressurization and entrapment of lubricant is the key theory that could explain microcracks growing; By the way, the role of lubricant and its effects are object of debates. It is suggested that the nucleation of pitting cracks is produced by penetration of oil into the microcracks (Bower 1988).

Bower (1988) has been one of the precursors to lay the foundations in pressurization and entrapment mechanism modeling. He modeled a shallow crack in 2D by analytical approach and proposed three types of model:

- Fluid lubricated crack faces (LCFM), in which the lubricant reduces only the friction between the crack faces and it does not exert pressure inside the cavity; μ_f=0.1;
- Fluid forced into the crack by the load (PM), that consists in applying on the crack faces a linear pressure distribution; In correspondence of the crack mouth, such pressure is equal to the contact pressure between the two mating bodies, and equal to zero on the crack tip;
- Fluid Entrapment Mechanism (ETM), in which the fluid is assumed to be blocked by the mating body; therefore the volume of fluid entrapped is kept constant into the cavity during the passage of the body.

Murakami (1985) considered the effect of the fluid from the point of view of crack opening displacement and oil seepage into the crack. From the results of a 3D model and experimental activities the following considerations could be drawn: (i) the effect of the fluid inside the cracks is to promote pitting-type wear, (ii) lubricant pressure in PM and ETM has been proven to extend the crack, respectively, towards the outer surface and the bulk material; other literatures as Bower (1988) and Datsyshyn (2001) confirm this; (iii) inclined cracks are most likely to trigger pitting and the most favourable situation is when the direction of the Hertzian load motion is in concordance with the crack inclination.

Makino (2012) investigated the consequences of RCF for the railway wheel steel. He attempted to interpret the experimental outcomes by using a 2D FEM model in ABAQUS which aimed to evaluate the SIF of an array of shallow cracks. In addition, the ETM has been taken in account, by hydrostatic elements, following the similar philosophy of Bower (1988).

More recently, Dallago et al. (2016) undertook a systematic investigation on the role of fluid entrapment and pressurization on the SIFs of inclined edge cracks as a function of friction coefficient, Hertzian pressure, Hertzian contact half-width, crack inclination angle. To reduce as much as possible the computational cost of the analyses, the second body was replaced with the theoretical Hertzian contact pressure distribution, thus neglecting the perturbation exerted by the cracked body on the contact pressure as well as the effect of the second body on the crack mouth displacement field. Pressurization and fluid entrapment mechanisms are combined sequentially: as the crack mouth opens, the contact pressure between the mating bodies, on the crack mouth, is uniformly transferred into whole crack cavity (PM); if the crack mouth is closed, the pressure inside the crack is the result of entrapment of lubricant inside (ETM). They concluded that the contribution of fluid entrapment (i) is more pronounced on Mode I than on Mode II, (ii) is negligible as long as the crack size is smaller than the contact half-width *a* and then suddenly increases and stabilizes as soon as the ratio crack size to contact half-width approaches the value of 2, (iii) is slightly favoured by higher crack inclination angles, although this effect is strongly dependent on the other parameters, (iv) is increased by friction, and (v) appears to be favoured by lower values of the contact load intensity.

This work is the prosecution and refinement of Dallago's model (Dallago (2016)); in particular, we aim at investigating the effect of the aforementioned simplifying assumptions. For this purpose, we model the actual contact between the mating bodies and include the entrapment mechanism ETM due to the closing action of the mating body on the crack mouth.

2. Pressurization model of Dallago et al.

This section introduces in detail the FE model of Dallago (2016). That was a reproduction of a linear 2D elastic plane having an edge crack, originally developed by Beghini et al. (2004) in ANSYS and validated with outcomes coming from literatures as Benedetti (2015). See the scheme in Fig. 1a. In order to model the contact between the faces and the crack closure, contact elements have been placed. For sake of lighter computational load, the contact with the second body is modelled by a Hertzian contact pressure distribution of half width *a* and maximum normal pressure centred in x with respect to the crack mouth (origin of the Cartesian reference system in Fig. 1a):

$$p(\xi) = p_{\max}\sqrt{1-\left(\frac{\xi - x}{a}\right)^2} \qquad \forall \xi \in [x-b, x+b] \tag{1}$$

where ξ is the coordinate on x-axis referred to crack mouth, aligned on with the half-plane. The friction forces *q*, caused by the contact between the two mating body, are hypothesised to follow the classical Coulombian law:

multiplying p by the friction coefficient μ_c; as result, the tangential tensions q own the same trend of distribution and point in the direction opposed to that of load's motion.

$$q(\xi) = \mu_c p(\xi) = \mu_c p_{\max} \sqrt{1 - \left(\frac{\xi - x}{a}\right)^2} \qquad \forall \xi \in [x-b, x+b] \tag{2}$$

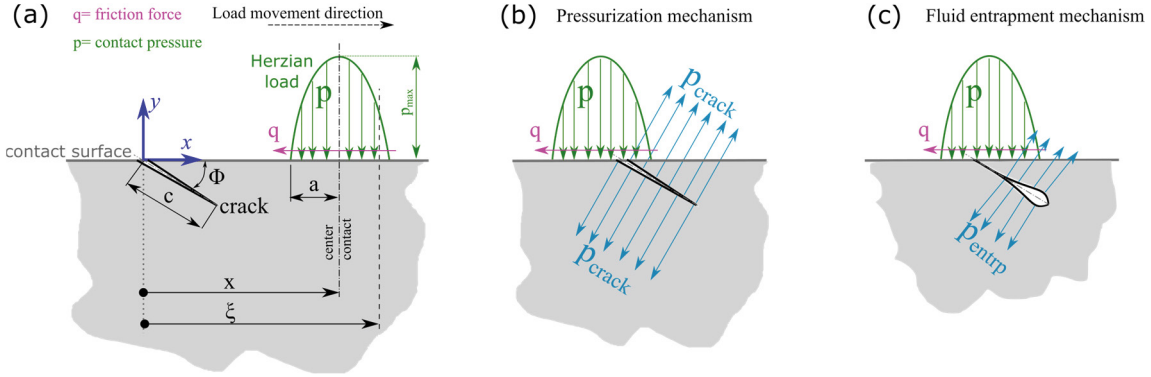

Fig.1. Schematic representation (a) of Dallago (2016) model: (b) pressurization mechanism phase and (c) entrapment mechanism;

Dallago et al. (2016) remark that the Hertzian load distribution is a strong simplification. But a time-consuming model, like that, would have never allowed the use of the required iterative procedures. As shown in Fig. 1a, the load travels from left to right (towards the positive direction of ξ), and the traction forces q are directed along the opposite direction. The friction coefficient between the crack faces μ_f is null because of the assumption of good lubrication and smoothing of the crack faces, due to their relative motion. The analyses of Dallago et al. have been classified in three categories:

- "dry" or well-lubricated analysis (LCFM), in which the fluid's pressure is neglected
- "wet" analysis, that considers the fluid to pressurize uniformly the whole cavity with a pressure p_{crack} equal to the contact pressure acting on the crack's mouth (PM) (see. Fig1b). This condition is valid as long as the crack faces remain open. As the contact load is able to close the lips of the crack mouth, despite the pressurization, the crack is considered closed (see Fig. 1c); form that position (named x_{cl}) on, p_{crack} is null. Therefore pressurization mechanism could be described by the following formula:

$$\begin{cases} p_{crack}(x) = 0 & \forall x \in [-\infty, -a] \\ p_{crack}(x) = p_{\max}\sqrt{1 - \left(\frac{x}{a}\right)^2} & \forall x \in [-a, x_{cl}] \quad x_{cl} \in [-a, a] \\ p_{crack}(x) = 0 & \forall x \in [x_{cl}, \infty] \end{cases} \tag{3}$$

- "entrapment" analysis, which is initially identical to the previous one; but from the position x_{cl} on is applied the pressure p_{entrp} due to the entrapment; considering the configuration in Fig.1c, v_{entrp} is defined as the volume of fluid enclosed into the cavity because the crack mouth's lips are tightened together by a exchange pressure of contact p_{clos}. At each position x, an iterative procedure looks for the p_{entrp} that maximises v_{entrp}; the upper bond condition is that v_{entrp} must be equal to or less than the value at the previous position, providing that the closure pressure p_{clos} is greater than p_{entrp}. In mathematical language is:

$$\begin{cases} \max\left(v_{entrp,i}\right) \\ v_{entrp,i} \le v_{entrp,i-1} \\ p_{entrp,i} < p_{clos,i} \end{cases} \tag{4}$$

where $v_{entrp,i}$, $p_{entrp,i}$ and $p_{closure,i}$ are, respectively, the v_{entrp} ,p_{entrp} and $p_{closure}$ at i-th position.

3. FE-model

The FE model of a 2D linear elastic plane has been used in the present work and is illustrated in Fig 4. The model is meant to reproduce a rotating rolling disk pressed against a semi-infinite flat plane body, in which prospective shallow crack has been inserted as geometrical discontinuity through the mesh (seam). The radius of the disk and its compressive load has been accurately chosen by analytical procedure in order to have an equivalent Hertzian contact of the experimental tribological system presented in Fontanari (2013) and Fontanari (2016).

Table 1. Experimental conditions of the rolling sliding wear test of Fontanari (2013).

Material	Young's modulus E	Poisson's ratio ν	Disks' diameter	Maximum Hertzian pressure p_{max}	Half-width of the contact area a	Friction coefficient μ_c
Tempered 42CrMo4V steel	205 GPa	0.3	26 and 54 mm	450 MPa	75μm	0.1

The crack tip region is modeled by collapsed quarter point singular elements and the SIFs are obtained by the near tip crack opening nodal displacements via the "Displacement Extrapolation Method" (Zhu (1995)). Such algorithm is supposed to be more accurate in this case because of the complex stress field. The FE-software used is ABAQUS 6.14. Free meshing technique has been adopted for this modeling because of flexibility in updating the geometry. By the way, it gives accuracy comparable with that achieved by mapped meshes. CPE6M elements with reduced integration are used. The simulations run in quasi-static conditions. The "General Contact" algorithm, with hard-contact property, is defined throughout the FE model, except for the contact between the crack's faces, in which the penalty surface-to-surface has been chosen. The friction coefficient between the two specimens is 0.1, and between the cracks faces is null because of the assumption of adequate internal lubrication. The disk translates parallel along the flat surface, and rotates about the centrum with angular velocity such that the experimental relative slide motion, in the work of Fontanari (2015), is reproduced. In few words, the direction of motion of the Hertzian load is opposite to the friction force. The elastic modulus E and Poisson's ratio ν are defined as 205GPa and 0.3, respectively.

The angle of inclination of the shallow crack with respect to the flat surface is chosen 25° in concordance with several models proposed by other authors (Makino (2012)) and the experimental evidences (Olver (2004)); in fact such configuration is most likely to be formed during the phase of initiation of cracks. Only a single crack is considered,

The effect of entrapment and evaluation of SIF is performed in the defect. Specifically, the blocking of the fluid into the crack has been assumed to be caused only by the closing action of the second body on the crack's mouth. Therefore, hydrostatic fluid elements have been exploited in order to simulate an ideal incompressible fluid entrapped in the cavity, defined by the crack faces and the surface of the disk. The hydrostatic elements maintain constant a target volume of the cavity operating on the pressure of the fluid in the cavity. In the first step of the simulation the second body is approaching the crack mouth Fig.2a. Then the system reaches the configuration such that the contact pressure of the disk over the crack mouth is enough to retain the fluid (Fig. 2b and Fig. 3a), from this

point on the volume of the fluid is imposed to be constant during the rest of simulation (Fig. 2c and Fig. 3b). There is also a successive moment in which the fluid is pushed out; see Fig. 2d. The present modeling follows the similar base concept of the fluid-entrapment-crack of Bower (1988) and Taizo Makino (2012).

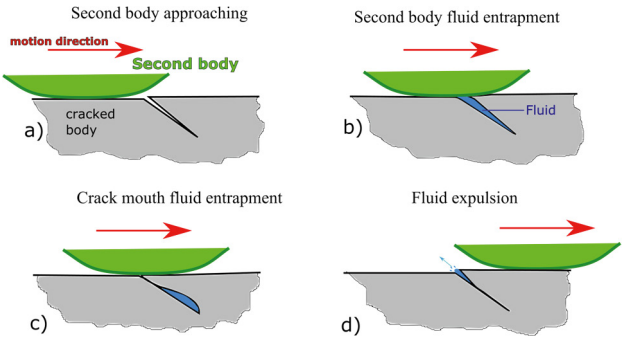

Fig.2. Approach of the second body: transition steps;

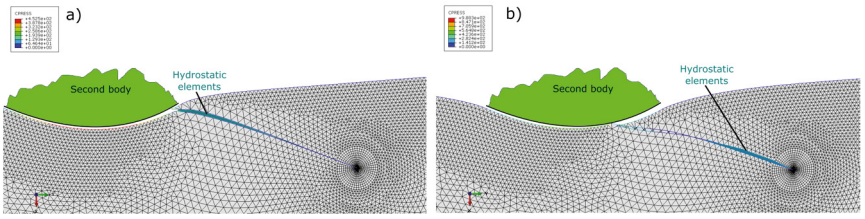

Fig. 3. Approaching instant of the second body on the crack mouth; hydrostatic element used in the simulation; the volume of the entrapped fluid has been conserved; the scale of deformations has been exaggerated for sake of clearness.

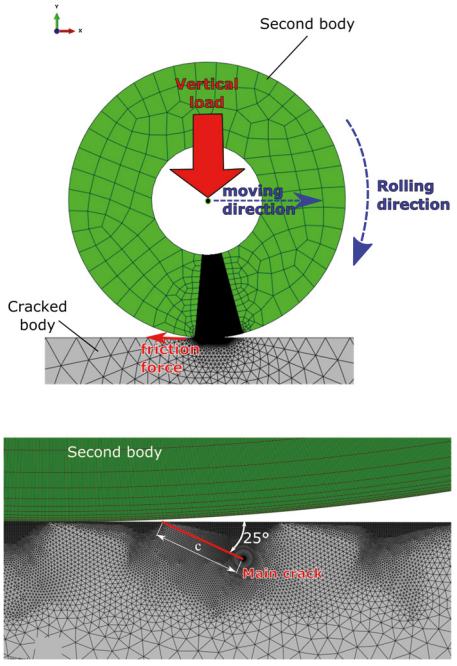

Fig. 4. Scheme of the FEM model; upon the global sight and downward the array of cracks.

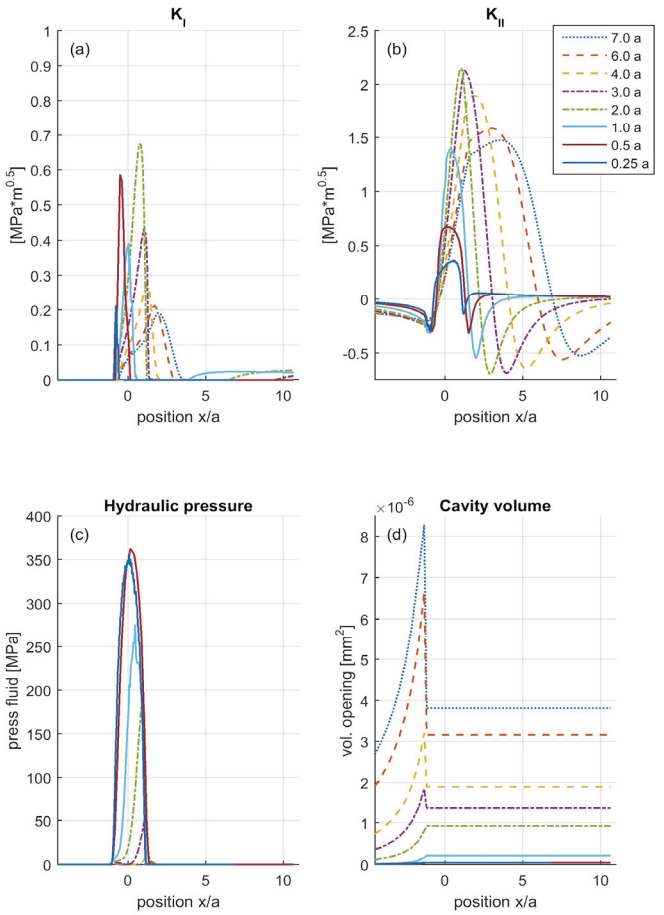

Fig. 5. Single crack: load cycles of SIF for different crack lengths; (a) K_I, (b) K_{II}, (c) p_c, (d) volume of crack cavity; a = 75μm, p_{max}=450MPa, E=210GPa, ν=0.3, μ_c=0.1, μ_f=0.0, Φ=25° ;

4. Results

4.1. Crack extension

The load cycles, using our FE model, corresponding to different crack lengths have been plotted in the Fig. 5. Globally, the magnitudes of *KI* are small in comparison with those of *KII*. It is clear that using this kind of approach the peak of hydraulic pressure p_c diminishes by extending the crack; but as long as the crack's dimension is short, the pressure curve reveals a quasi-similar trend to the Hertzian distribution. Obviously, the longer a crack is and the greater is the volume of the cavity. Generally, *KII* curves show a similar trend: initially there is a small negative peak, they reach a significant positive peak and then *KII* is reversed and shows a second negative peak. Increasing the crack length, the variation of *KII* becomes larger; but after the length of *2a*, the trend is reversed; maybe, the reason is that the crack tip is getting farther from the zone of high stresses.

4.2. Comparison with pressurization model of Dallago

It is worth of interest the comparison of the present outcomes with Dallago's model (Dallago 2016).

Firstly, the case of crack having length *c=0.5a*, shown in Fig. 6 is exanimated. The SIFs differ significantly during the PM phase in which *KI* is larger and *KII* has a relevant negative peak. The entrapment mechanism of the present model does not exert remarkable opening action in comparison with PM. Comparing hydraulic pressure curve of the present model with Dallago's one, the first is rightward shifted and the peak is quite lower.

Analysing a longer crack *c=4a*, shown in Fig. 7, the deviation between the two models becomes larger. Increasing the crack length, the opening action is amplified during PM, but it diminishes for the ETM.

Bower (1988) has already doubted the reliability of PM modeling, because the estimation of crack growth rate by Paris' law is not in agreement with the practical evidence.

Observing the evolution of the hydraulic pressure as a function of the position of the contact load shown in Fig. 6, it is quite interesting to notice that the two models of entrapment and pressurization of Dallago are similar for short cracks. It is thus possible to hypothesize that for short cracks the pressurization model is an acceptable approximation of the entrapment model. The careful reader could object that there is a deviation between the hydraulic pressures, but this can be explained in the following way. The pressure of the fluid for the entrapment mechanism depends on the stress state along the entire length of the crack, while that for the pressurization mechanism coincides with the contact pressure at the crack mouth. The classical Hertzian theory informs us that the contact stresses decrease steadily from the surface towards the bulk, thus it is obvious that longer cracks experience weaker average compressive stress fields along their faces and, as a consequence, lower hydraulic pressures. The contrary is evidently also true. These considerations allow us to state that as the length of the crack is progressively decresed a quasi-uniform stress field of compression is obtained throughout the crack that tends to approach the maximum value at the mouth. Therefore, the intensity of the peak in hydraulic pressure for the entrapment mechanism approaches that produced by the pressurization mechanism. Obviously the subsurface stresses are slightly lower than those on the contact surface and the occurrence of the flaw modifies the theoretical stress distribution.

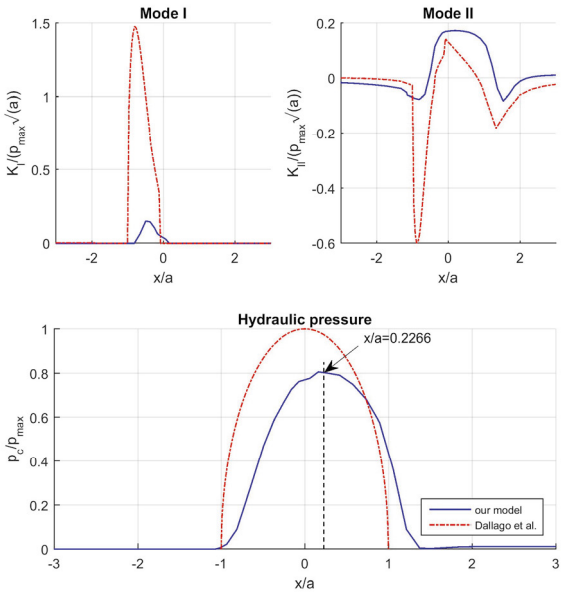

Fig. 6. Comparison of our model with those of Dallago (2016) with pressurization mechanism plus entrapment; normalized SFI in mode I and mode II versus normalized Hertzian load center position volume of crack cavity; Single crack, c/a=0.5, $p_{max}/E\approx0.0026$, $\nu=0.3$, $\mu_c=0.05$, $\mu_f=0.0$, $\Phi=25°$;

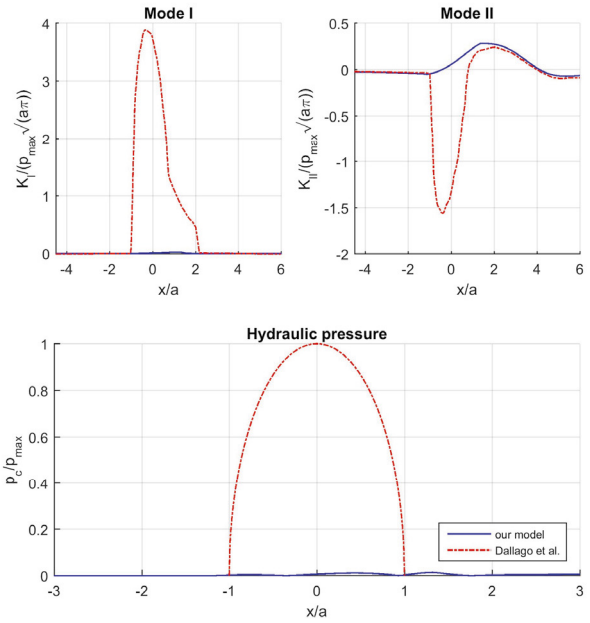

Fig. 7. Comparison of our model with those of Dallago (2016) with pressurization mechanism plus entrapment; normalized SFI in mode I and mode II versus normalized Hertzian load centre position volume of crack cavity; Single crack, c/a=4, $p_{max}/E\approx0.0026$, $\nu=0.3$, $\mu_c=0.05$, $\mu_f=0.0$, $\Phi=20°$;

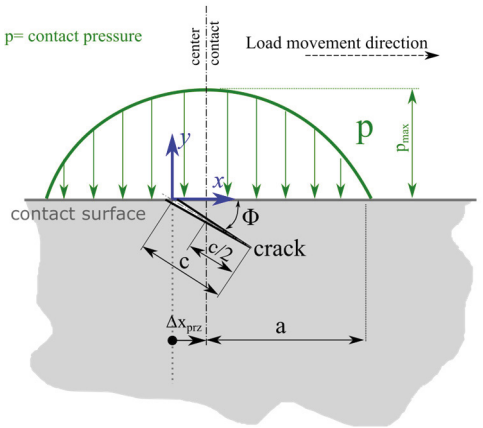

Fig. 8. Configuration of maximal pressurization due to entrapment for short crack

In addition, it is reasonable to assume that the maximum hydraulic pressure occurs at the point where the maximum contact pressure lays on the middle of the segment defined by the projection of the crack on the contact surface, as in this configuration a greater fraction of the crack is embedded in the contact stress field (see Fig. 8); this is valid on condition that the crack is small with respect to *a* and the surrounding stress field is approximately homogenous. This can be expressed by the following formula:

$$\Delta x_{prz} = \frac{c \cdot \cos(\Phi)}{2} \qquad c << a \tag{5}$$

In fact, for $c=0.5a$, $\Delta x_{prz}/a$ is equal to 0.2266 which is in agreement with the plot shown in Fig. 6.

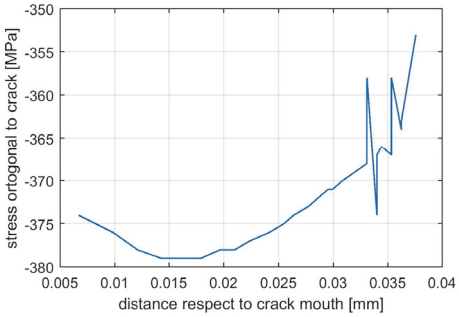

Fig. 9. Stress orthogonal to the crack face vs distance respect to the crack mouth for $c=0.5a$ and $x/a=0.2266$.

The normal component of the tensor, orthogonal and near to the crack faces, has been plotted for different values of distance respect to crack mouth, see Fig. 9. The stress distribution for the crack $c=0.5a$, shows the state of compression in the neighborhood, and it may explain the magnitude of the hydraulic pressure.

4.3. Considerations of SIF intensity

Considering the scale magnitude of the intensity factors in exam, the crack is not supposed to propagate, because it does not overpass the characteristic threshold of the material. See Fig. 5. As result, according to the traditional model of Paris, the pitting wear should not come up and yet it does; see Fontanari (2013) and Fontanari (2015). Bower (1988) has already faced this dilemma. Follow up, that the criterion of crack propagation should be revised for the contact fatigue.

5. Conclusions

A FE-model has been realised in order to interpret numerically the experimental pitting phenomena. The entrapment has been modelled, as Bower (1988) and Makino (2012), assuming the blockage of the fluid to be promoted only by the contact of the foreign body on the crack mouth. Then the present outcomes have been compared with those coming from pressurization model of Dallago (2016). The following conclusions could be drawn:

- The coplanar extension of the crack reduces the effect of fluid entrapment.
- By using only fluid entrapment mechanism, the SIF in mode I is low in comparison with the one in mode II; however, it likely the crack to propagate in mode II in this conditions;
- Imposing pressurization pressure into the cavity, equal to the contact pressure on the crack mouth (pressurization mechanism of Dallago) overestimates SIF in mode I respect to the present model;
- For short cracks, the fluid pressure curves for entrapment and pressurization mechanism show similar trends; we stress on the fact that they differ in a small shift and in slight reduction of the maximal value of pressure.
- The law of crack propagation should be revised for contact fatigue; it is likely for the thresholds in rolling contact fatigue to be lower.

References

Bower, A.F., 1988. The influence of crack face friction and trapped fluid on surface initiated rolling contact fatigue cracks, J. Tribology ASME 110(4), 704-711

Beghini, M., Bertini, L., Fontanari, V., 2004. Parametric study of oblique edge cracks under cyclic contact loading, Fatigue Fract Engng Mater Struct 28, 31–40

Bogdanski, S., Olzak, M., Stupnicki, J., 1996. Numerical stress analysis of rail rolling contact fatigue cracks, Wear 191, 14-24.

Bogdanski, S., Stupnicki, J., Brown, M.W., Cannon, D.F., 1997. A Two Dimensional Analysis of Mixed Mode Rolling Contact Fatigue Crack Growth in Rails, 5th International Conference on Biaxial/Multiaxial Fatigue and Fracture, Cracow.

Bogdanski, S., Lewicki, P., 2008. 3D model of liquid entrapment mechanism for rolling contact fatigue cracks in rails, Wear 265, 1356–1362

Dallago, M., Benedetti, M., Ancellotti, S., Fontanari, V., 2016 (in press). The role of lubricating fluid pressurization and entrapment on the path of inclined edge cracks originated under rolling–sliding contact fatigue: Numerical analyses vs. experimental evidences, International Journal of Fatigue.

Datsyshyn, O.P., Panasyuk, V.V., 2001. Pitting of the rolling bodies contact surface, Wear 251, 1347–1355.

Fletcher, D. I., Beynon, J. H., 1999. A simple method of stress intensity factor calculation for inclined fluid-filled surface-breaking cracks under contact loading, Proceedings of the Institution of Mechanical Engineers 213, Part J, 299-304.

Fletcher, D.I., Hyde, P., Kapoor, A., Modelling and full-scale trials to investigate fluid pressurization of rolling contact fatigue cracks, Wear 265 (2008), pp. 1317–1324

Fontanari, V., Benedetti, M., Straffelini, G., Girardi, Ch., Giordanino, L., 2013. Tribological behavior of the bronze–steel pair for worm gearing. Wear 302, 1520–7.

Fontanari, V., Benedetti, M., Girardi, Ch., Giordanino, L., 2016. Investigation of the lubricated wear behavior of ductile cast iron and quenched and tempered alloy steel for possible use in worm gearing. Wear.

Kaneta, M., Murakami, Y., Yatsuzuka, H., 1985. Mechanism of Crack Growth in Lubricated Rolling/Sliding Contact, ASLE Transactions 28(3), 407-414.

Kaneta, M., Murakami, Y., 1987. Effects of oil hydraulic pressure on surface crack growth in rolling/sliding contact, Tribology International 20(4), 210-217.

Keer, L.M., Bryant, M.D., Haritos, G.K., 1982. Subsurface and surface cracking due to Hertzian contact, Journal of Lubrication Technology 104(3), 347-351

Keer, L.M., Bryant, M.D., 1983. A pitting model for rolling contact fatigue, Journal of Lubrication Technology 105(2), 198-205

Makino, T., Kato, T., Hirakawa, K., 2012. The effect of slip ratio on the rolling contact fatigue property of railway wheel steel, International Journal of Fatigue, 36(1), 68-79.

Murakami, Y., Kaneta, M., Yatsuzuka, H., 1985. Analysis of Surface Crack Propagation in Lubricated Rolling Contact, ASLE Transactions 28(1), 60-68.

Olver, A. V., 2005. The Mechanism of Rolling Contact Fatigue: An Update, Proceedings of the Institution of Mechanical Engineers, Part J: Journal of Engineering Tribology 219(5), 313-330.

Ren, Z., Glodez, S., Fajdiga, G., Ulbin, M., 2002. Surface initiated crack growth simulation in moving lubricated contact. Theoret. Appl Fract Mech 38, 141–9.

Ringsberg, J. W., Bergkvist, A., 2003. On propagation of short rolling contact fatigue cracks, Fatigue Fract Engng Mater Struct 26, 969-98.

Roberts, R., 1971. Mode II fatigue propagation, Journal of basic Engineering, Trans ASME, 671-680

Sadeghi, F., Jalalahmadi, B., Slack, T.S., Arakere, N.K., 2009. A review of rolling contact fatigue. J Tribol 131, 041403.

Zhu, W.X., Smith, D.J., 1995. On the use of displacement extrapolation to obtain crack tip singular stresses and stress intensity factors. Eng Fract Mech 51(3), 391–400.